Direct Measurements of Conformer-Dependent Reactivity of the Criegee Intermediate CH_3CHOO

Craig A. Taatjes *et al.*

Science **340**, 177 (2013);
DOI: 10.1126/science.1234689

Science (print ISSN 0036-8075; online ISSN 1095-9203) is published weekly, except the last week in December, by the American Association for the Advancement of Science, 1200 New York Avenue NW, Washington, DC 20005.

Direct Measurements of Conformer-Dependent Reactivity of the Criegee Intermediate CH_3CHOO

Craig A. Taatjes,[1]* Oliver Welz,[1] Arkke J. Eskola,[1] John D. Savee,[1] Adam M. Scheer,[1] Dudley E. Shallcross,[2] Brandon Rotavera,[1] Edmond P. F. Lee,[3,4] John M. Dyke,[3] Daniel K. W. Mok,[4] David L. Osborn,[1] Carl J. Percival[5]*

Although carbonyl oxides, "Criegee intermediates," have long been implicated in tropospheric oxidation, there have been few direct measurements of their kinetics, and only for the simplest compound in the class, CH_2OO. Here, we report production and reaction kinetics of the next larger Criegee intermediate, CH_3CHOO. Moreover, we independently probed the two distinct CH_3CHOO conformers, syn- and anti-, both of which react readily with SO_2 and with NO_2. We demonstrate that *anti*-CH_3CHOO is substantially more reactive toward water and SO_2 than is *syn*-CH_3CHOO. Reaction with water may dominate tropospheric removal of Criegee intermediates and determine their atmospheric concentration. An upper limit is obtained for the reaction of *syn*-CH_3CHOO with water, and the rate constant for reaction of *anti*-CH_3CHOO with water is measured as $1.0 \times 10^{-14} \pm 0.4 \times 10^{-14}$ centimeter^3 second^{-1}.

Ozonolysis of alkenes is generally understood to proceed via a 1,3-cycloaddition of ozone across the olefinic bond to produce a primary ozonide, the decomposition of which forms a carbonyl moiety and a Criegee intermediate (CI) (*1*). The fate of the CI determines the end products of the ozonolysis reaction and can have a substantial impact on the atmosphere (*1*–*4*). Recently, the simplest CI, CH_2OO, has been directly produced in the gas phase with low internal energies from reaction of O_2 with CH_3SOCH_2 (*5*, *6*) or CH_2I (*4*, *7*, *8*) and unambiguously detected by tunable synchrotron or laser photoionization mass spectrometry. These techniques allowed direct measurements of the reaction kinetics of CH_2OO with several important tropospheric species, including SO_2 and NO_2, both of which react much faster with CH_2OO than models had assumed (*4*). Since those direct measurements appeared, new high-level calculations (*9*), field measurements (*10*), and ozonolysis experiments (*10*–*12*) continue to suggest that CI reactions are important in tropospheric sulfate chemistry. However, substantial uncertainty remains, partly because of the absence of direct kinetic measurements of any larger CI and partly because of uncertainty in the products of CI reactions. Moreover, the reactivity of larger CIs is predicted to be affected by the nature and location of the substituents (*13*), with a particularly large effect for the crucial reaction of CI with water (*13*, *14*). Because of the large amount of water in Earth's atmosphere, the rate of CI removal by water is a key determinant of the tropospheric impact of all CI reactions. Determining the conformer dependence of CI reactions is therefore not only a vital aspect of understanding their fundamental reactivity, it is also a key component for improving atmospheric chemistry models.

We have successfully extended our earlier technique of reacting α-iodoalkyl radicals with O_2 to prepare CIs (*4*, *7*, *15*), and here we show that the reaction of the 1-iodoethyl radical (CH_3CHI) with O_2 forms both conformers of the CI acetaldehyde oxide (CH_3CHOO) at 298 K and 4 torr. The conformers of acetaldehyde oxide, *syn*-CH_3CHOO and *anti*-CH_3CHOO, differ in the orientation of the C-O-O group (depicted in Fig. 1). By taking advantage of the difference in ionization energy of the two conformers, we demonstrate a dramatic conformer dependence of CH_3CHOO reactivity toward SO_2 and H_2O.

Kinetic measurements were carried out in the Multiplexed Chemical Kinetics Reactor, which has been described in detail elsewhere (*4*, *16*, *17*). Reactions are initiated by pulsed laser photolysis in a slow-flow reactor. The contents are continuously sampled through a small orifice in the reactor and probed by photoionization time-of-flight mass spectrometry. Ionizing with tunable photon energy, from the Chemical Dynamics Beamline (9.0.2) of the Advanced Light Source, allows isomers to be distinguished on the basis of their photoionization spectra (*17*–*19*). The reaction of CH_3CHI with O_2 shows similar behavior to the reaction of CH_2I with O_2, with the most prominent products being the stabilized CI. (CH_3CHOO), an I atom, and secondary products IO and HOI. (A time-resolved mass spectrum of the reaction initiated by photolysis of CH_3CHI_2 in the presence of oxygen is displayed in fig. S2.)

The mass/charge (m/z) = 60 signal is identified as the CI, acetaldehyde oxide, on the basis of its exact mass and a comparison of its photoionization spectrum with a predicted spectrum derived from ab initio calculations (*19*) of both the adiabatic ionization energy (AIE) and Franck-Condon factors for photoionization of both conformers of CH_3CHOO, as shown in Fig. 1. Detailed results of these calculations are given in the supplementary text.

Calculations place the syn conformer ~15 kJ mol^{-1} lower in energy than *anti*-CH_3CHOO (*14*). Reflecting the zwitterionic character of the C–O bond, the barrier to interconversion of these conformers is substantial (*14*), ~160 kJ mol^{-1}. Therefore, *syn*- and *anti*-CH_3CHOO act as distinct chemical species at atmospheric temperatures. The syn and anti conformers of CH_3CHOO also have different photoionization spectra. In the threshold region, each conformer has ionization transitions to both A″ and A′ cationic states, and the

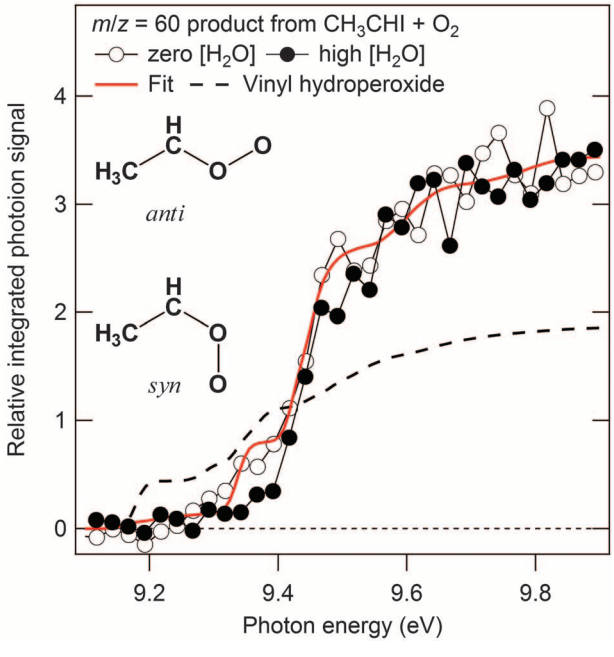

Fig. 1. The photoionization spectrum for the m/z = 60 product from photolysis of CH_3CHI_2 in the presence of O_2. The best fit of the zero-water trace to the calculated photoionization spectra for *syn*- and *anti*-CH_3CHOO is also shown. The fit allows the the energies for the excited (A′) cationic state of each conformer to vary within a range of ~50 meV about their calculated values. The black dashed line shows the calculated photoionization spectrum of vinyl hydroperoxide. Addition of water preferentially removes the anti conformer, as seen in the decreased signal between 9.3 and 9.4 eV for the high-H_2O trace.

[1]Combustion Research Facility, Mail Stop 9055, Sandia National Laboratories, Livermore, CA 94551–0969, USA. [2]School of Chemistry, University of Bristol, Bristol BS8 1TS, UK. [3]School of Chemistry, University of Southampton, Highfield, Southampton SO17 1BJ, UK. [4]Department of Applied Biology and Chemical Technology, The Hong Kong Polytechnic University, Hung Hom, Hong Kong. [5]School of Earth, Atmospheric and Environmental Sciences, The University of Manchester, Williamson Building, Oxford Road, Manchester M13 9PL, UK.

*Corresponding author. E-mail: cataatj@sandia.gov (C.A.T.); Carl.Percival@manchester.ac.uk (C.J.P.)

calculated four photoionization bands overlap (fig. S4). Allowing a small adjustment to the computed ionization energies for each conformer gives a very close fit to the observed spectrum (Fig. 1). The low-energy edge of the spectrum is dominated by the anti conformer, which can be detected below the ionization energy of the syn conformer. Assuming that the electronic transition moments for the two conformers are similar, the fit parameters suggest a far larger overall production (90%) of the more stable syn conformer. The signals observed at higher ionizing photon energies will be dominated by photoionization of *syn*-CH_3CHOO (supplementary text). The two conformers are independently detected, but their ratio is not varied in these experiments.

Acetaldehyde oxide has several other isomers (scheme S1), most of which have ionization energies well above the threshold observed for the m/z = 60 product of the reaction of CH_3CHI with O_2, including acetic acid, the AIE of which is 10.70 eV, and methyl formate, with an AIE of 10.85 eV (*20*). Only vinyl hydroperoxide has a low enough calculated AIE, 9.18 eV, to be considered as a carrier for the m/z = 60 product spectrum. However, the predicted ionization onset and Franck-Condon envelope of vinyl hydroperoxide (Fig. 1) is not consistent with the observed spectrum.

Vinyl hydroperoxide is calculated to be the dominant product of isomerization from *syn*-CH_3CHOO, with a calculated barrier to isomerization of >80 kJ mol^{-1} (*21*). [Isomerization of *anti*-CH_3CHOO is more likely to lead to methyl dioxirane (*21*), with a calculated AIE of 10.36 eV.] The O–O bond in vinyl hydroperoxide is weak (*22*), and fission of that bond is a pathway to formation of OH in ozonolysis reactions (*23*). In fact, recent multireference calculations predict extremely rapid dissociation of vinyl hydroperoxide after isomerization from CH_3CHOO (*24*).

The first-order decay rate of CH_3CHOO in the absence of additional reactants is the sum of unimolecular and heterogeneous loss reactions. The decay depends on the coating of the reactor, suggesting that heterogeneous reaction contributes substantially. The slowest decay observed in this context, ~250 s^{-1}, is an upper limit to the thermal (298 K) rate coefficient for decomposition of CH_3CHOO, consistent with the determination of 76 s^{-1} by Fenske *et al.* (*25*). Upon adding SO_2 or NO_2 as reagent, the decay of the CH_3CHOO signal becomes more rapid (shown in Fig. 2 for SO_2 reaction with CH_3CHOO). A linear fit of the decay constant versus reactant concentration measured at photon energies where photoionization of the syn conformer dominates (Fig. 3 and fig. S5) returns as its slope $k_{1,syn}$, the second-order rate coefficient for the reaction of *syn*-CH_3CHOO with SO_2 (uncertainty limits are 95%):

$$\textit{syn}\text{-}CH_3CHOO + SO_2 \rightarrow \text{products}$$
$$k_{1,syn} = 2.4 \times 10^{-11} \pm 0.3 \times 10^{-11}\ cm^3\ s^{-1} \quad (1)$$

A similar plot measured with 9.37-eV photons, where photoionization of the *anti*-CH_3CHOO conformer dominates (open symbols in Fig. 3), yields a rate coefficient more than twice as large,

$$\textit{anti}\text{-}CH_3CHOO + SO_2 \rightarrow \text{products}$$
$$k_{1,anti} = 6.7 \times 10^{-11} \pm 1.0 \times 10^{-11}\ cm^3\ s^{-1} \quad (2)$$

Similar measurements on the overall reaction of *syn*- and *anti*-CH_3CHOO with NO_2 (described in supplementary text) suffer from reduced signal-to-noise ratio but show a rate coefficient of $2 \times 10^{-12} \pm 1 \times 10^{-12}$ cm^3 s^{-1}, with a slight (statistically significant at 1σ confidence interval) conformer dependence. This rate coefficient is substantially smaller than that for CH_2OO reacting with NO_2, $k(CH_2OO + NO_2) = 7 \times 10^{-12}$ cm^3 s^{-1} (*4*).

The rapid reaction of CH_3CHOO with SO_2 supports predictions of barrierless addition of SO_2 to CI (*9*, *26*, *27*) and indicates that the reactions of CI with SO_2 should be generally facile. The substantial difference in reactivity between *syn*- and and *anti*-CH_3CHOO may partly reflect increased steric hindrance for formation of the CI-SO_2 secondary ozonide in the syn conformation or conformer-selective electron donating effects from the methyl group, as theoretically described, for example, in the $CH_3CHOO + H_2O$ reaction (*13*). The rate coefficient for *syn*-CH_3CHOO reaction with SO_2 is slightly smaller than that measured earlier for CH_2OO reacting with SO_2 [$k(CH_2OO + SO_2) = 3.9 \times 10^{-11} \pm 0.7 \times 10^{-11}$ cm^3 s^{-1}] (*4*), but that for *anti*-CH_3CHOO is larger. Both are orders of magnitude larger than estimates typically used in tropospheric models (*28*).

Measurements have also been carried out at higher ionizing photon energies (13 eV), where

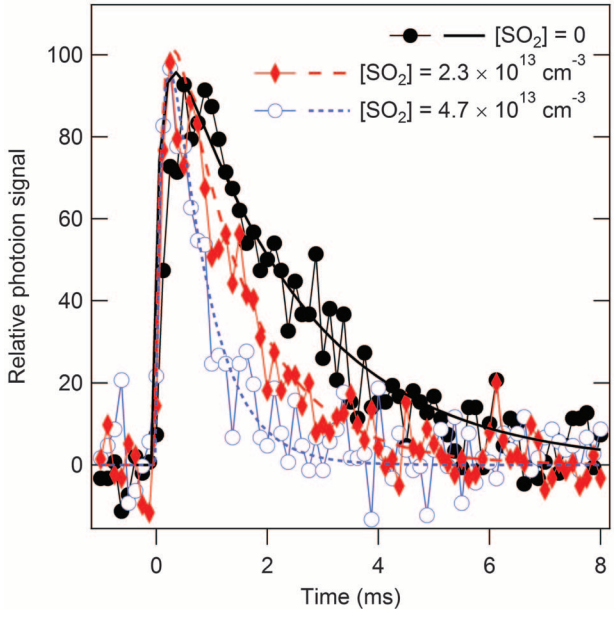

Fig. 2. Representative time-dependent CH_3CHOO signals. The time behavior of the m/z = 60 signal (mainly from ionization of *syn*-CH_3CHOO) from photolysis of CH_3CHI_2 in the presence of SO_2 and $[O_2] = 1.2 \times 10^{16}$ cm^{-3}, measured with Lyman-α radiation at 10.2 eV.

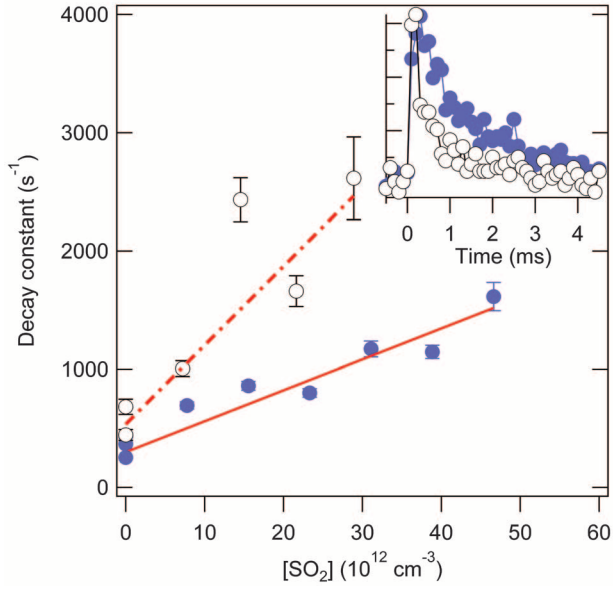

Fig. 3. Rate coefficients for reaction of CH_3CHOO conformers with SO_2. Fitted pseudo–first-order decay constants of *syn*-CH_3CHOO (solid circles) and *anti*-CH_3CHOO (open circles) are shown as a function of SO_2 concentration. The lines are linear fits to the data, weighted by the statistical uncertainty in the exponential fit to the individual decay traces (±1σ error bars shown in the figure). Each fit included >20 points across the relevant decay. **(Inset)** The decay of CH_3CHOO measured with 10.50 eV (solid circles, predominantly syn) and 9.37 eV (open circles, predominantly anti) in the presence of $[SO_2] = 7.2 \times 10^{12}$ cm^{-3}.

the SO_3 co-product [AIE of 12.81 eV (*29*)] can be directly observed. To within the experimental uncertainty, SO_3 is formed with a rise time that correlates with the decay time of the CI (figs. S6 to S9), showing that SO_3 is a direct product of the reactions of both CH_2OO and CH_3CHOO with SO_2. Vereecken *et al.* (*9*), improving on earlier calculations (*26*, *27*), predicted that formation of SO_3 and a carbonyl compound will be the principal product channel for small CIs and at low pressure but that stabilization of a CI-SO_2 secondary ozonide becomes dominant for larger CIs under atmospheric conditions. Under the conditions of the present experiments, no stabilized CI-SO_2 product is observed for either CH_2OO or CH_3CHOO reaction with SO_2. The eventual fate of the CI-SO_2 secondary ozonide may determine the relevance of CI reactions with SO_2 to tropospheric sulfate chemistry and particulate formation, and will affect the interpretation and intercomparison of laboratory ozonolysis experiments that are sensitive to either CI consumption or H_2SO_4 formation (*10*–*12*).

Because reaction with water dominates tropospheric CI removal (*9*), its rate constant is critical to modeling the CI concentration. The reaction of CH_2OO with water is too slow to measure in the present apparatus (*4*), and only an upper limit could be obtained, 4×10^{-15} cm^3 s^{-1}. However, the reaction of water with CH_3CHOO is predicted to favor the anti conformer by five orders of magnitude (*13*), and indeed (Fig. 1) the addition of H_2O preferentially depletes the photoionization spectrum at the low-energy edge, where *anti*-CH_3CHOO dominates. Measurements of CH_3CHOO with 10.5-eV photons in the presence of H_2O concentrations of 2.4×10^{16} cm^{-3} showed an identical decay to those with no added water, suggesting similar upper limits for the reaction of water with *syn*-CH_3CHOO and with CH_2OO: 4×10^{-15} cm^3 s^{-1} (*4*). However, a significant and systematic increase in the decay rate with water addition was observed for measurements with 9.37-eV photons (Fig. 4), permitting direct measurement of the rate coefficient (uncertainty limits are 95%),

$$\textit{anti}\text{-}CH_3CHOO + H_2O \rightarrow \text{products}$$
$$k_{3,anti} = 1.0 \times 10^{-14} \pm 0.4 \times 10^{-14}\ cm^3\ s^{-1} \quad (3)$$

This result is more than a factor of 10 below the high-pressure limiting rate coefficient from the transition state theory predictions of Anglada *et al.* (*13*), $k_{3,anti} = 1.68 \times 10^{-13}$ cm^3 s^{-1} but is a factor of 35 above the prediction of Kuwata *et al.* (*14*), $k_{3,anti} = 2.87 \times 10^{-16}$ cm^3 s^{-1}. In any case, the rate coefficient is substantially larger than that calculated for other CI reactions with water and tends to validate the theoretical prediction of a dramatic lowering of the activation energy for the anti conformer (*13*, *14*). Because the reaction is predicted to proceed by stabilization (supplementary text), it is possible that the rate coefficient is pressure dependent. Master-equation calculations, including accurate treatment of the association kinetics, would give the most rigorous comparison for the present experiments.

We emphasize that the low-pressure rate coefficients measured here for reactions of the CIs with SO_2, NO_2, and water are lower limits for the total removal of CI by these species at the higher pressures of the troposphere or laboratory ozonolysis experiments. Furthermore, even in cases where the CI removal is independent of pressure, the products may change substantially with pressure (*9*). Interpretation of indirect measurement of CI reactions often depends on product detection and on derived yields of stabilized CI in ozonolysis that are in turn based on inferences about CI scavenger reactions. Apparent discrepancies among indirect determinations, for example, for reactions of CI with SO_2 (*10*–*12*), may be related to that web of inference. The present measurements break the connection to ozonolysis, directly producing stabilized CIs in a nearly thermoneutral reaction, characterizing the Criegee reactant by its photoionization spectrum, and determining absolute rate constants by pseudo–first-order kinetics methods. Comparing indirect measurements to the present direct kinetics determinations may therefore provide a means to refine the detailed modeling of ozonolysis.

Moreover, computed rate coefficients for substituted CI calculated by state-of-the-art quantum chemistry and advanced theoretical kinetics (*9*, *30*) will be of increasing importance in the development of chemical models for complex systems such as atmospheric chemistry. The present results are a benchmark for such calculations and will enable a more rigorous understanding of CI chemistry and a more accurate description of the role of CI in the troposphere.

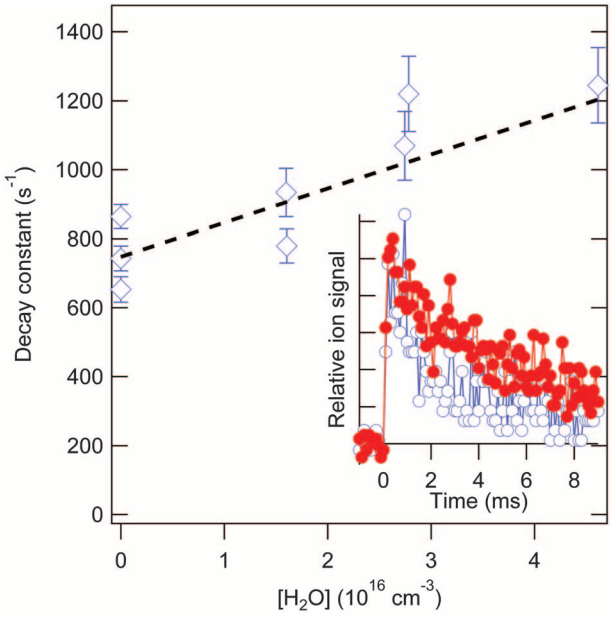

Fig. 4. Rate coefficient for reaction of *anti*-CH_3CHOO with H_2O. Fitted pseudo–first-order decay constants of *anti*-CH_3CHOO are shown as a function of H_2O concentration. The dashed line is a fit to the data, weighted by the statistical uncertainty in the exponential fits to the individual decay traces (±1σ error bars shown in the figure). Each fit included >20 points across the relevant decay. **(Inset)** The decay of CH_3CHOO measured with 10.50 eV (solid circles, predominantly syn) and 9.37 eV (open circles, predominantly anti) in the presence of [H_2O] = 2.7×10^{16} cm^{-3}.

References and Notes

1. D. Johnson, G. Marston, *Chem. Soc. Rev.* **37**, 699 (2008).
2. R. M. Harrison *et al.*, *Sci. Total Environ.* **360**, 5 (2006).
3. S. Gäb, E. Hellpointner, W. V. Turner, F. Korte, *Nature* **316**, 535 (1985).
4. O. Welz *et al.*, *Science* **335**, 204 (2012).
5. R. Asatryan, J. W. Bozzelli, *Phys. Chem. Chem. Phys.* **10**, 1769 (2008).
6. C. A. Taatjes *et al.*, *J. Am. Chem. Soc.* **130**, 11883 (2008).
7. C. A. Taatjes *et al.*, *Phys. Chem. Chem. Phys.* **14**, 10391 (2012).
8. J. M. Beames, F. Liu, L. Lu, M. I. Lester, *J. Am. Chem. Soc.* **134**, 20045 (2012).
9. L. Vereecken, H. Harder, A. Novelli, *Phys. Chem. Chem. Phys.* **14**, 14682 (2012).
10. R. L. Mauldin 3rd *et al.*, *Nature* **488**, 193 (2012).
11. P. T. M. Carlsson, C. Keunecke, B. C. Krüger, M.-C. Maaß, T. Zeuch, *Phys. Chem. Chem. Phys.* **14**, 15637 (2012).
12. T. Berndt *et al.*, *J. Phys. Chem. Lett.* **3**, 2892 (2012).
13. J. M. Anglada, J. González, M. Torrent-Sucarrat, *Phys. Chem. Chem. Phys.* **13**, 13034 (2011).
14. K. T. Kuwata, M. R. Hermes, M. J. Carlson, C. K. Zogg, *J. Phys. Chem. A* **114**, 9192 (2010).
15. H. Huang, A. J. Eskola, C. A. Taatjes, *J. Phys. Chem. Lett.* **3**, 3399 (2012).
16. D. L. Osborn *et al.*, *Rev. Sci. Instrum.* **79**, 104103 (2008).
17. C. A. Taatjes *et al.*, *Phys. Chem. Chem. Phys.* **10**, 20 (2008).
18. C. A. Taatjes *et al.*, *Science* **308**, 1887 (2005); 10.1126/science.1112532.
19. Materials and methods are available as supporting materials on *Science* Online.
20. D. A. Sweigart, D. W. Turner, *J. Am. Chem. Soc.* **94**, 5592 (1972).
21. J. M. Anglada, J. M. Bofill, S. Olivella, A. Solé, *J. Am. Chem. Soc.* **118**, 4636 (1996).
22. N. Sebbar, H. Bockhorn, J. W. Bozzelli, *Phys. Chem. Chem. Phys.* **5**, 300 (2003).
23. N. M. Donahue, G. T. Drozd, S. A. Epstein, A. A. Presto, J. H. Kroll, *Phys. Chem. Chem. Phys.* **13**, 10848 (2011).
24. T. Kurtén, N. M. Donahue, *J. Phys. Chem. A* **116**, 6823 (2012).
25. J. D. Fenske, A. S. Hasson, A. W. Ho, S. E. Paulson, *J. Phys. Chem. A* **104**, 9921 (2000).
26. L. Jiang, Y. S. Xu, A. Z. Ding, *J. Phys. Chem. A* **114**, 12452 (2010).
27. T. Kurtén, J. R. Lane, S. Jørgensen, H. G. Kjaergaard, *J. Phys. Chem. A* **115**, 8669 (2011).
28. M. E. Jenkin, S. M. Saunders, M. J. Pilling, *Atmos. Environ.* **31**, 81 (1997).
29. D. S. Alderdice, R. N. Dixon, *J. Chem. Soc., Faraday Trans. II* **72**, 372 (1976).
30. L. Vereecken, J. S. Francisco, *Chem. Soc. Rev.* **41**, 6259 (2012).

Acknowledgments: Additional pseudo–first-order rate constants, details of the experiments and calculations, and spectroscopic data underpinning this work are presented in the supplementary materials. The participation of O.W., A.J.E., J.D.S., D.L.O., and C.A.T. and the development of the experimental kinetics apparatus were funded by the Division of Chemical Sciences, Geosciences, and Biosciences, the Office of Basic Energy Sciences, the U.S. Department of Energy. D.E.S., J.M.D., and C.J.P. thank the Natural Environment Research Council for funding, and J.M.D. thanks the Leverhulme Trust for a senior fellowship. The Advanced Light Source is supported by the Director, Office of Science, Office of Basic Energy Sciences, of the U.S. Department of Energy under contract DE-AC02-05CH11231 at Lawrence Berkeley National Laboratory. Sandia is a multiprogram laboratory operated by Sandia Corporation, a Lockheed Martin Company, for the National Nuclear Security Administration under contract DE-AC04-94-AL85000. D.K.W.M., J.M.D., C.J.P., and E.P.F.L. acknowledge support from the Research Grant Council of the Hong Kong Special Administrative Region (grant no. Polyu 5019/11P) and the National Service for Computational Chemistry Software (UK) for computational resources. The experiments were conceived by C.A.T., C.J.P., and D.E.S.; designed by C.A.T., D.L.O., C.J.P., O.W., and A.J.E.; and carried out by O.W., J.D.S., A.J.E., A.M.S., B.R., C.J.P., C.A.T., and D.L.O. E.P.F.L., D.K.W.M., and J.M.D. were responsible for the quantum chemistry and Franck-Condon calculations. All authors participated in the data analysis and interpretation and contributed to the manuscript.

Supplementary Materials
www.sciencemag.org/cgi/content/full/340/6129/177/DC1
Materials and Methods
Supplementary Text
Figs. S1 to S19
Schemes S1 and S2
Tables S1 to S8
References (*31*–*49*)

2 January 2013; accepted 15 February 2013
10.1126/science.1234689

Enantioselective Synthesis of Pactamycin, a Complex Antitumor Antibiotic

Justin T. Malinowski,* Robert J. Sharpe,* Jeffrey S. Johnson†

Medicinal application of many complex natural products is precluded by the impracticality of their chemical synthesis. Pactamycin, the most structurally intricate aminocyclopentitol antibiotic, displays potent antiproliferative properties across multiple phylogenetic domains, but it is highly cytotoxic. A limited number of analogs produced by genetic engineering technologies show reduced cytotoxicity against mammalian cells, renewing promise for therapeutic applications. For decades, an efficient synthesis of pactamycin amenable to analog derivatizations has eluded researchers. Here, we present a short asymmetric total synthesis of pactamycin. An enantioselective Mannich reaction and symmetry-breaking reduction sequence was designed to enable assembly of the entire carbon core skeleton in under five steps and control critical three-dimensional (stereochemical) functional group relationships. This modular route totals 15 steps and is immediately amenable for structural analog synthesis.

Complex organic molecules produced by bacteria have been used to treat numerous disease types for nearly a century (*1*–*4*). However, many naturally derived compounds that exhibit interesting bioactivities are practically inaccessible via synthetic organic chemistry. A natural product's structural complexity can create an insurmountable impediment to the preparation of analogs that might exhibit improved characteristics. An ongoing challenge in the field of synthetic chemistry is the development of methods that close the gap between the efficiency of biosynthetic machinery and laboratory synthesis. Because of the inherent flexibility of the latter, success in this endeavor could provide access to useful structural variants that might otherwise be inaccessible.

Pactamycin (**1**; Fig. 1) was isolated from *Streptomyces pactum* var. *pactum* in 1961 by Argoudelis *et al*. (*5*). The bioactivity profile of this natural product is especially notable, as it displays antitumor, antimicrobial, antiviral, and antiprotozoal properties by acting as a universal inhibitor of translocation (*6*–*9*). Within the ribosomal subunit in which it interacts, pactamycin mimics an RNA dinucleotide through interactions of its aniline and salicylate moieties with stem loops in the 16*S* RNA (*10*). Unfortunately, pactamycin's therapeutic benefits have yet to be realized, due to high cytotoxicity (median inhibitory concentration of 95 nM against human diploid embryonic cell line MRC-5) (*11*). Pactamycin is a prototypical example of a promising bioactive natural product whose complexity hampers the investigation of structure-activity relationships (SARs) that might lead to a serviceable therapeutic application and/or a better understanding of intrinsic bioactivity.

Genetic engineering studies have reignited promise for medicinal application, as 7-deoxy– and 8″-hydroxy–derivatives were isolated and displayed diminished cytotoxicity (*11*–*14*). In the context of the work described herein, it is worth noting that Lu *et al*. contend that the structural complexity of **1** renders these and related structural modifications "inaccessible by synthetic organic chemistry" (*12*). Conversely, we have proceeded from the hypothesis that the genetic engineering approach to pactamycin analogs might be inherently limited by the biosynthetic machinery (*15*, *16*). Though pactamycin is commercially available, a chemical approach to its synthesis could, in principle, provide far greater opportunity and flexibility for discovering and advancing useful compounds. However, this tactic will only be feasible in the presence of an efficient synthesis platform that rapidly develops the appropriate level of structural complexity. In fact, synthetic interest in pactamycin has recently flourished, culminating in the landmark 32-step total synthesis from Hanessian and co-workers (*17*, *18*), as well as numerous partial synthetic studies (*19*–*23*). Despite these creative, state-of-the-art approaches, a compelling case can be made that a more practical synthesis solution is needed.

In this Report, we disclose a 15-step total synthesis of pactamycin, which has, in the initial pass, produced the natural product on a milligram scale and a key branch-point intermediate on a gram scale. We emphasized both modular construction and introduction of functionality in the final desired form of pactamycin, enabling an approach amenable to derivatization for analog synthesis. Late-stage introduction of the aniline- and salicylate-binding elements provides an opportunity for future SAR studies.

The recognition of a hidden symmetry in the northeast quadrant of pactamycin (**1**) was critical to our synthetic plan. Depicted in Fig. 2A, the carbon chain connecting C-4 and C-8 can be extracted to a symmetrical α-ureido-2,4-pentanedione **2**. We envisaged simplified formation of the fully substituted C-1 center via a Mannich reaction. Due to the symmetrical methyl ketone substituents at C-1, diastereoselectivity considerations are obviated, allowing for a focus on the enantioselective C-2–amino incorporation during the C-1–C-2 bond construction. The nascent C-2 stereocenter would then need to direct a site- and diastereoselective diketone monoreduction, setting the C-2/C-1/C-7 stereotriad (red dashed arrows in Fig. 2B). This sequence would provide the entire pactamycin carbon-core skeleton from which modular delivery of various functionality (Fig. 2C) could provide **1** and/or its congeners in rapid fashion.

The first challenge we faced was implementation of the Mannich reaction with an appropriately configured imine electrophile. We were encouraged by results reported by Schaus and co-workers,

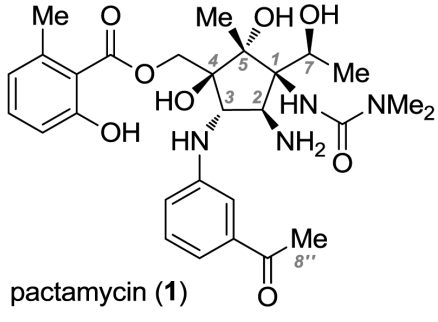

Fig. 1. Structure of pactamycin (1). Me, methyl.

Department of Chemistry, University of North Carolina at Chapel Hill, Chapel Hill, NC 27599, USA.

*These authors contributed equally to this work.
†Corresponding author. E-mail: jsj@unc.edu